Journal of Sound and Vibration 330 (2011) 883–901

Contents lists available at ScienceDirect

Journal of Sound and Vibration

journal homepage: www.elsevier.com/locate/jsvi

Suppression of maglev vehicle–girder self-excited vibration using a virtual tuned mass damper

D.F. Zhou [a,*], C.H. Hansen [b], J. Li [a]

[a] Maglev Engineering Center, National University of Defense Technology, Changsha 410073, China
[b] School of Mechanical Engineering, The University of Adelaide, SA 5005, Australia

ARTICLE INFO

Article history:
Received 15 March 2010
Received in revised form
20 September 2010
Accepted 20 September 2010
Handling Editor: J. Lam
Available online 16 October 2010

ABSTRACT

The self-excited vibration that occurs between a stationary Electromagnetic Suspension (EMS) maglev vehicle and a girder is a practical problem that greatly degrades the performance of a maglev system. As of today, this problem has not been fully solved. In this article, the principle underlying the self-excited vibration problem is explored, and it is found that the fundamental resonance frequency of the maglev girder plays a vital role in the initiation of the self-excited vibration. To suppress the self-excited vibration, a scheme applying a tuned mass damper (TMD) to the maglev girder is proposed, and the stability of the combined system is analyzed. Furthermore, a novel concept of a virtual TMD is introduced, which uses an electromagnetic force to emulate the force of a real TMD acting on the girder. However, in the presence of the time delay caused by the inductance of the electromagnets, the stability analysis of the levitation system combined with the virtual TMD becomes complex. Analysis of the stability shows that there exist some repeated time delay zones within which the overall system is stable. Based on this rule, time delay control is introduced to stabilize the system with a virtual TMD, and a procedure to determine the optimal time delay and gain is proposed. Numerical simulation indicates that the proposed virtual TMD scheme can significantly suppress the self-excited vibration caused by one unstable vibration mode, and is suitable for application to EMS maglev systems.

1. Introduction

The maglev train is a novel guideway transportation system that is currently under rapid development around the world. Compared with conventional railway systems, the maglev system has the advantages of low noise and high speed, since there is no mechanical contact between the vehicle and the guideway, which makes the maglev system suitable for long distance as well as urban transportation. Until today, two commercial maglev routes, as well as several test routes, have been established around the world [1]. Among these routes, most of them are the Electromagnetic Suspension (EMS) type.

The EMS maglev system uses electromagnetic attractive forces to neutralize the gravity of the vehicle, and active control is required to stabilize the suspension system around a desired suspension gap because the magnetic attraction suspension by itself is inherently unstable. As a result, coupled vibration problems associated with the vehicle and guideway in an EMS maglev system are more complex than those that occur in a conventional railway system. Recently,

* Corresponding author. Tel.: +86 731 84573387x8103; fax: +86 84516000.
E-mail address: Danf.Zhou@gmail.com (D.F. Zhou).

0022-460X/$ - see front matter © 2010 Elsevier Ltd. All rights reserved.
doi:10.1016/j.jsv.2010.09.018

a comprehensive review of the coupled vibration problems in EMS maglev systems has been done by Zhou et al. [2]. They classified coupled vibration problems into three categories: stationary vehicle–guideway self-excited vibration, moving vehicle–bridge coupled vibration, and vehicle–guideway interaction caused by track irregularities. The stationary vehicle–guideway self-excited vibration is a unique phenomenon that occurs only in EMS maglev systems, and it can be further divided into two subclasses: stationary electromagnet–track self-excited vibration and stationary vehicle–bridge self-excited vibration. The moving vehicle–guideway coupled vibration problem has been extensively studied by Yau [3,4]; however, relatively little attention has been paid in the literature to the stationary vehicle–guideway self-excited vibration problem, which occurs when the EMS maglev vehicle is suspended above an elevated girder without moving, and which is the subject of concern in this paper.

It has been observed that when the self-excited vibration occurs, the amplitude of the vertical vibration of the girder grows with time until the electromagnets clash with the surface of the track, leading to a levitation failure. This problem greatly degrades the performance of the maglev system and is unacceptable for a commercial maglev system, since it hinders the vehicle from stopping at an arbitrary location along the route. For example, She et al. [5] pointed out that the TR08 high speed maglev vehicle on the Shanghai maglev demonstration line had experienced violent coupled vibration while the vehicle was crossing a turnoff at a very low speed. Their research indicates that the parameters of the girder, including its first-order natural frequency and damping ratio, play an important role in the stability of the coupled vibration problem.

Albert et al. [6] pointed out that the American Maglev Technologies (AMT) system achieved successful levitation in Florida on a guideway mounted to the earth on a concrete foundation, but later encountered difficulties in achieving stable levitation when the vehicle was moved to a guideway installed on the Old Dominion University campus. It was believed that the flexibility of the guideway on the Old Dominion University campus, which employed 90-feet long, essentially simply supported elevated girders, was the main reason that contributed to the difficulties of achieving a stable levitation.

Yet as of today, to the authors' knowledge, no control method that can solve the stationary self-excited vibration problem in a real maglev system has been reported. The purpose of the research reported here is to develop a vibration control method that is capable of eliminating the self-excited vibration and is applicable to a real maglev system.

The tuned mass damper (TMD) has been widely used to reduce the vibration of flexible structures. Its application to bridges for the purpose of reducing the vibration caused by moving vehicles has been extensively discussed [7,8]. It has been shown that if the parameters of the TMD are well tuned, the performance of the TMD is excellent. However, the application of a TMD to a maglev girder for the purpose of suppressing the stationary vehicle–girder self-excited vibration has not yet been reported in the literature. The feasibility and stability of this application is considered in this paper.

Recently, the virtual vibration absorber, which uses an actuator to emulate the force of a real TMD, has been introduced by Wu and Shao [9] and Wu et al. [10,11]. In their research, the stiffness of the virtual TMD was tuned online by an adaptation algorithm that managed to keep the phase error between the acceleration of the primary body and the displacement of the virtual mass within a desired range. The feasibility of this scheme had been verified by both simulation and experiments. This concept is also suitable for application to EMS maglev systems, since the electromagnets in an EMS maglev vehicle, by themselves, are excellent actuators. Yet the stability problem associated with using a virtual TMD needs to be investigated, and an adaptive algorithm to tune the parameters of the TMD needs to be developed and this is the focus of the current paper.

When the force of a real TMD is emulated by an electromagnetic force, some special characteristics need to be taken into account. A factor that greatly affects the stability of the system is the time delay caused by the dynamics of the electromagnets. Generally, the inductance of an electromagnet in a low speed maglev train can be up to 0.1 H and it varies with the levitation gap and track materials; therefore, the time delay between the input voltage and the output attraction force should not be neglected in the implementation of a virtual TMD. It is well known that a time delay may decrease the stability margin of a closed loop control system or even cause the system to become unstable. Wang et al. [12] investigated the magnetic levitation system with delayed gap feedback control, and showed that as the time delay in the gap feedback path exceeds a critical value, a pair of complex poles cross the imaginary axis, and the stability of the levitation system may change through a Hopf bifurcation. Hence, compensation for actuation time delay in the maglev system is essential for the successful application of the virtual TMD.

To minimize the influence resulting from the time delay associated with the actuator, some compensation methods have been proposed by others. For example, the time delay of hydraulic actuators has been taken into account in the vibration control of a building under seismic excitation [13,14]. A general compensation method used in this problem is to predict the displacement, x_1, of the actuator after a specified time delay τ, and then compute the current control signal using the predicted displacement x_1. Here, τ equals the time delay of the actuator, which is a constant in their study [13]. Since the time delay exists in the actuation, following the time delay τ, the resulting displacement of the actuator, x_1', should be almost identical to the predicted displacement x_1. A neural network controller of a vibration reduction system for a tall building was proposed by Nikzad et al. [14]. The neural network was trained in a laboratory setup before it was put into use. Experimental comparison of the proposed neural network method and the conventional feedforward controller (which was generally made up of two first-order phase lead compensators) showed that the neural network controller performed better in compensating for actuation time delay than the feedforward controller did. The neural network is also adopted by Dong et al. [15] to compensate the uncertain time delay of the magneto-rheological dampers of car suspension systems. However, neither the phase lead compensator nor the neural network compensator is suitable for

use in compensating the actuation force lag in a maglev train—the phase lead compensators are easy to apply but can only provide limited phase compensation over a limited frequency band; the neural network may provide adequate phase compensation if well trained, but the success of the training process greatly depends on the extent of the experiences that the network is exposed to during the training period, and is computationally expensive.

In this study, the virtual TMD scheme is applied, for the purpose of suppressing the maglev vehicle–girder self-excited vibration. To neutralize the effect of the actuation time delay, an additional time delay, τ_1, is introduced in the virtual TMD feedback paths. Together with the actuation time delay, τ_0, if the overall time delay, $\tau_0+\tau_1$, equals one or more cycles of vibration, the additional electromagnetic force will be in phase with the estimated TMD force; thus, the vibration will be suppressed. The stability of this scheme is investigated here and it will be shown that there exist a series of time delay intervals within which the additional time delay can be chosen to stabilize the coupled system. The advantage of this scheme is obvious: the time delay of the actuator can be used as part of the control delay and it is insensitive to noise and external disturbances. The proposed vibration control scheme provides a method to analyze the stability of the vehicle–girder coupled system, as well as a solution to solve the stationary self-excited vibration problem.

The reminder of this article is organized as follows: First, the models of the magnetic levitation system as well as the flexible maglev girder are established, and the stability of the coupled system is analyzed in Section 2. In Section 3, the application of the TMD to a maglev girder is introduced, and the stability of the coupled system together with the TMD is investigated. The realization of the virtual TMD is presented in Section 4, in which the actuation time delay issue and its affect on the stability of the closed loop system are discussed. Based on the discussion, the time delay control strategy is introduced, and a procedure to determine the optimal time delay and gain is proposed. To verify the effectiveness of the procedure, a numerical simulation is conducted in Section 5, followed by a brief conclusion in Section 6.

2. Stability analysis of the electromagnet–girder coupled system

2.1. Modeling of the magnetic levitation system and the flexible girder

For an actual maglev vehicle, the magnetic levitation system consists of several bogies, with each bogie supported by at least four electromagnets. A side view of the CMS-03A low speed maglev vehicle is shown in Fig. 1(a), from which it can be seen that the weight of the car body is supported by four bogies, with each bogie consisting of eight electromagnets (four on each side); therefore, there are a total of 32 electromagnets in the vehicle. Each pair of adjacent electromagnets is controlled by one controller; thus, there are a total of 16 levitation units in a single vehicle. As the levitation unit is the basic element of the maglev vehicle, solving the stability problem of a single levitation unit-girder coupled system is

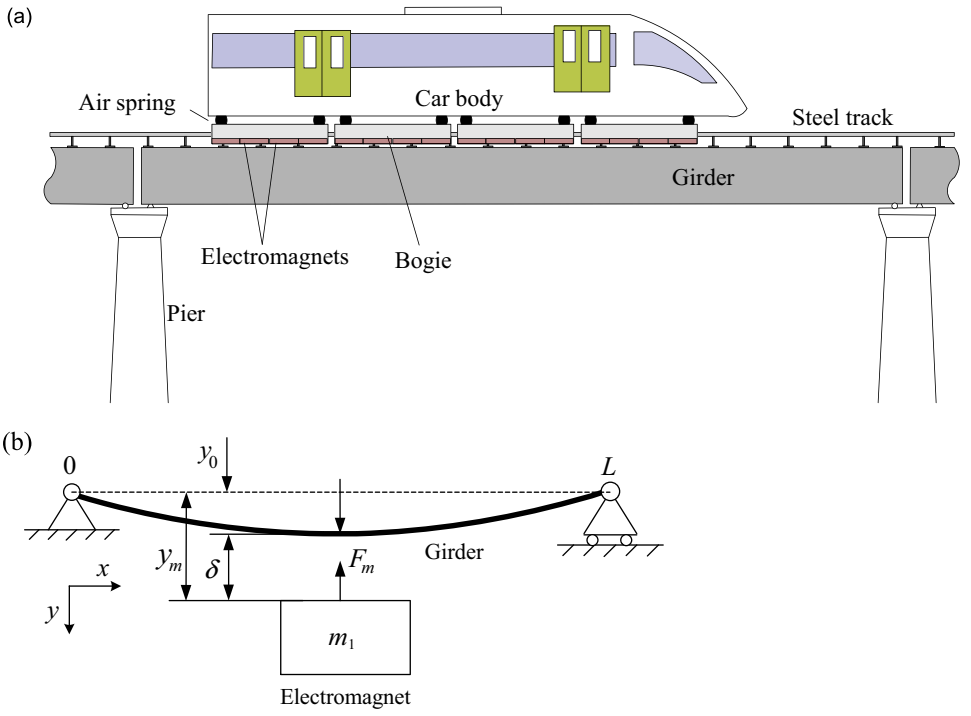

Fig. 1. Schematic of the electromagnetic levitation system: (a) side view of the CMS03A low speed EMS maglev vehicle and (b) simplified electromagnet–girder coupled model.

essential to ensure the stability of the vehicle–girder coupled system. Without loss of generality, several assumptions are made when developing the dynamic model of the maglev vehicle:

(a) The levitation units are mechanically decoupled by the bogie and the stability of one levitation unit is not affected by other levitation units.
(b) The secondary suspension system of the vehicle can be neglected in the analysis, since the air springs isolate the vibration of the levitation system from the car body.
(c) The girder in a maglev route is generally simply supported, and it can be modeled as a Bernoulli–Euler beam, because in most cases the length of the girder is large compared with other dimensions and the deflections of the bridges are small compared with their length.
(d) The length of the electromagnet can be neglected when compared with the span length of a maglev girder; the nonlinearity of the girder response is not considered because the amplitude of the vibration is generally quite small (several millimeters) compared with the span length of a girder (typically 18 or 24 m, or even longer) and is thus well below the amplitude at which nonlinear effects would be significant.

The schematic of a single levitation unit-girder coupled system is shown in Fig. 1(b), in which the electromagnet is simplified as a lumped mass, m_1. Let N denote the number of turns of a single electromagnet, and suppose that the area of the magnetic pole is A, the space permeability is μ_0, and the gap between the electromagnet and the lower surface of the steel track is δ. Referring to Fig. 1(b), it can be seen that $\delta = y_m - y_0$. Then the magnetic flux through the U-shaped iron core of the electromagnet, ϕ, is given by

$$\phi = \frac{\mu_0 A N i(t)}{2\delta(t)}, \tag{1}$$

where $i(t)$ is the current through the coil of the electromagnet. A levitation unit consists of two electromagnets in series; therefore, for a single electromagnet, the relationship between the control voltage u and the current i can be described as

$$\frac{u(t)}{2} = i(t)R + N\frac{d\phi(t)}{dt}, \tag{2}$$

where R is the direct current (DC) resistance of a single electromagnet. Substituting Eq. (1) into Eq. (2), yields:

$$\frac{u(t)}{2} = i(t)R + \frac{\mu_0 A N^2}{2\delta(t)}\dot{i}(t) - \frac{\mu_0 A N^2 i(t)}{2\delta^2(t)}\dot{\delta}(t). \tag{3}$$

It can be shown that the electromagnetic force, F_m, generated by the two electromagnets is given by [3,4,12]

$$F_m(t) = \frac{\mu_0 A N^2}{2}\left(\frac{i(t)}{\delta(t)}\right)^2. \tag{4}$$

Therefore, the motion of the electromagnet can be expressed as follows:

$$m_1\frac{d^2 y_m}{dt^2} = -F_m(t) + m_1 g. \tag{5}$$

Here g is the acceleration due to gravity. Combining Eqs. (4) and (5), the steady-state current (when the term in the left hand side of Eq. (5) equals zero) can be obtained as

$$i_0 = \sqrt{\frac{2m_1 g z_0^2}{\mu_0 A N^2}}. \tag{6}$$

An additional controlling force should be applied to stabilize the levitation system since the magnetic levitation system by itself is inherently unstable. Here, the widely applied PD controller [2] is adopted, which gives:

$$i_e(t) = k_p[\delta(t) - z_0] + k_d\dot{y}_m(t), \tag{7}$$

where z_0 is the desired levitation gap, which is a constant in most cases; i_e is the desired current, and k_p and k_d are the proportional and derivative control coefficients, respectively. Eq. (7) is an ideal control law. Taking the inductance of the electromagnets into account, a proportional control law can be applied to adjust the control voltage and to approximately generate the desired control current:

$$u(t) = k_c[i_e(t) - i(t)], \tag{8}$$

where k_c is the proportional control coefficient. This control scheme not only minimizes the lag of the responding current, but also provides a relatively clear physical meaning—the output of the PD controller is the desired control current through the electromagnets, which also provides facilities for combining a virtual TMD into the closed control system. This will be demonstrated in the following sections.

Suppose that the span length of the girder is L, the mass per unit length and the bending stiffness of the bridge are ρ and EI, respectively, and the displacement of the girder is $y(x,t)$. Then the motion of the girder can be described by the following

differential equation:

$$EI\frac{\partial^4 y(x,t)}{\partial x^4}+\rho\frac{\partial^2 y(x,t)}{\partial t^2}=f(x,t), \tag{9}$$

where $f(x,t)$ is the external force acting on the girder, which can be approximately described as

$$f(x,t)=F_m(t)\delta(x-x_0), \tag{10}$$

where x_0 is the location of the electromagnet, and $\delta(\cdot)$ is the Dirac delta function. For a simply supported girder, the displacement of the girder can be described as a superposition of sinusoidal functions:

$$y(x,t)=\sum_{n=1}^{\infty} y_n(t)\sin\frac{n\pi x}{L}. \tag{11}$$

Substituting Eq. (11) into Eq. (9), multiplying both sides of the resultant equation by $\sin(n\pi x/L)$, and integrating both sides from 0 to L, gives:

$$\ddot{y}_n(t)+\omega_n^2 y_n(t)=\frac{2F_m}{\rho L}\sin\frac{n\pi x_0}{L},\quad n=1,2,\ldots, \tag{12}$$

where

$$\omega_n=\left(\frac{n\pi}{L}\right)^2\sqrt{\frac{EJ}{\rho L}}. \tag{13}$$

Eq. (12) can be interpreted as a series of dynamic equations for single degree of freedom (sdof) mass–spring resonators. The equivalent mass of the nth mass–spring resonator is

$$\overline{m}_n=\frac{\rho L}{2}\csc\frac{n\pi x_0}{L}. \tag{14}$$

Here, $\csc(\cdot)$ is the cosecant function. Consequently, the equivalent stiffness of the sdof resonator can also be obtained, which is

$$\overline{k}_n=\frac{EJ}{2}\left(\frac{n\pi}{L}\right)^4\csc\frac{n\pi x_0}{L}. \tag{15}$$

By analogy to the sdof system, the mechanical impedance of the nth vibration mode of the girder can be defined as

$$Z_n=\sqrt{\overline{k}_n\overline{m}_n}=\frac{\sqrt{EJ\rho L}}{2}\left(\frac{n\pi}{L}\right)^2\csc\frac{n\pi x_0}{L}\geq\frac{\sqrt{EJ\rho L}}{2}\left(\frac{n\pi}{L}\right)^2. \tag{16}$$

It can be seen that the mechanical impedance is proportional to n^2, which implies that the higher the order of the vibration mode, the larger will be the mechanical impedance, and thus a smaller response will occur for the same external excitation force. Therefore, the higher order vibration modes are not easily excited, which coincides with the observation in practice that the self-excited vibration always occurs at a frequency corresponding to either the fundamental resonant mode of a girder or the first harmonic.

According to Eq. (11), the displacement of the girder at the location where the electromagnet is levitating can be obtained as

$$y_0(t)=y(x_0,t)=\sum_{n=1}^{\infty} y_n(t)\sin\frac{n\pi x_0}{L}. \tag{17}$$

Inspections of Eqs. (12) and (17) reveal that the girder can be modeled as a series of undamped sdof mass–spring resonators of different but related resonance frequencies, with each resonator corresponding to a particular vibration mode of the girder. Therefore, the stability of the electromagnet–girder coupled system can be investigated by separately examining the stability of each sdof resonator–electromagnet coupled system. If all the sdof resonator–electromagnet coupled systems are stable, the overall system is stable; otherwise, if one of them is unstable, the overall system is unstable, and self-excited vibration will occur.

Based on practical considerations, the first-order mode of the girder is examined here. The location of the electromagnet is chosen as $L/2$, which corresponds to the worst case since when $x_0=L/2$, the mechanical impedance, Z_1, reaches its minimum value. Under these assumptions, the displacement of the girder at $x=L/2$ is

$$y_0(t)=y_1(t) \tag{18}$$

and the dynamic equation of the girder, described by Eq. (12), becomes

$$\ddot{y}_0(t)+\omega_1^2 y_0(t)=\frac{2F_m(t)}{\rho L} \tag{19}$$

or

$$m_0\ddot{y}_0(t)+k_0 y_0(t)=F_m(t), \tag{20}$$

where m_0 and k_0 is the equivalent mass and stiffness of the first-order vibration mode, and $m_0=\overline{m}_1=\rho L/2$, $k_0=\overline{k}_1=(EI/2)(\pi/L)^4$.

Combining Eq. (20) with Eqs. (3)–(5) and (7)–(8), the dynamic behavior of the closed loop system can be determined. When examining the stability of the coupled system around the equilibrium point, the linearized model can be applied to simplify the analysis without introducing noticeable errors. The linearized model is given by

$$\begin{cases} u=k_pk_c(y_m-y_0-z_0)+k_dk_c\dot{y}_m \\ L_0\dot{i}=u/2-iR+F_i(\dot{y}_m-\dot{y}_0) \\ F_m=2(F_ii-F_z(y_m-y_0)) \\ m_1\ddot{y}_m+F_m=0 \\ m_0\ddot{y}_0+k_0y_0=F_m \end{cases}, \tag{21}$$

where

$$L_0=\frac{\mu_0AN^2}{2z_0},\quad F_i=\frac{\mu_0AN^2i_0}{2z_0^2},\quad F_z=\frac{\mu_0AN^2i_0^2}{2z_0^3}.$$

2.2. Stability analysis of the coupled system

The coupled system described by Eq. (21) can be decomposed into two subsystems in a negative feedback interconnection as shown in Fig. 2: the levitation system, $G_0(s)$, and the sdof mass–spring system, $H(s)$. $G_0(s)$ is defined as the transfer function between the electromagnetic force acting on the girder and the excitation, v_0. Here, s is the Laplace operator, and v_0 is the vertical velocity of the girder at location x_0, which equals$\dot{y}_0$and is positive when the girder is moving downwards. Since the electromagnetic force, F_m, is equal in strength to the force acting on the girder, but is opposite in direction, the output of $G_0(s)$ is $-F_m$. $H(s)$ is defined as the transfer function between the responding velocity of the girder and the excitation force acting on it. In the model, F_d is the external force disturbances acting on the girder, such as the wind induced disturbance and the levitation forces produced by other levitation units. The negative feedback in the loop indicates that the nominal direction of the electromagnetic force, F_m, is opposite in direction to the force acting on the girder.

According to Fig. 2 and Eq. (21), and using $v_0=\dot{y}_0$, the transfer function of $G_0(s)$ can be deduced using the first four equations in Eq. (21):

$$G_0(s)=-\frac{F_m(s)}{v_0(s)}=\frac{\eta m_1 s}{m_1L_0s^3+m_1\overline{R}s^2+F_ik_ck_ds+\eta} \tag{22}$$

and $H(s)$ can be obtained from the last equation of Eq. (21)

$$H(s)=\frac{v_0(s)}{F_0(s)}=\frac{s}{m_0s^2+k_0}, \tag{23}$$

where $\overline{R}=R+k_c/2$, and $\eta=F_ik_ck_p-2F_z\overline{R}$, which are both constants. It is a basic requirement that the levitation system by itself is stable, namely, all the eigenvalues of the system described by Eq. (22) must have negative real parts, which requires that $m_1\overline{R}F_ik_ck_d>m_1L_0\eta$, and $\eta>0$. Therefore, the requirements for the control parameters are: $k_ck_d>(\eta L_0/F_i\overline{R})$ and $k_ck_p>(2F_z\overline{R}/F_i)$.

The characteristic polynomial of the coupled system is

$$\Delta(s)=1+G_0(s)H(s), \tag{24}$$

which can be rewritten using Eqs. (22) and (23) as

$$\Delta(s)=m_0m_1L_0s^5+m_0m_1\overline{R}s^4+(m_1L_0k_0+F_ik_ck_dm_0)s^3+[k_0m_1\overline{R}+\eta(m_0+m_1)]s^2+F_ik_0k_ck_ds+\eta k_0. \tag{25}$$

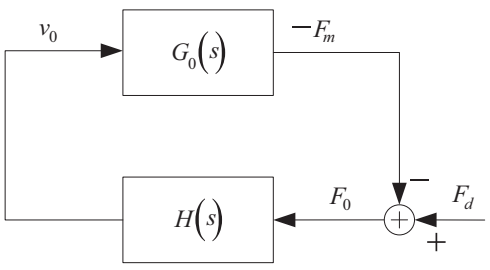

Fig. 2. Block diagram of the closed loop system. It can be divided into two subsystems.

Table 1
Routh array of the closed loop system.

s^5	$m_0 m_1 L_0$	$m_1 L_0 k_0 + F_i k_c k_d m_0$	$F_i k_0 k_c k_d$
s^4	$m_0 m_1 \overline{R}$	$k_0 m_1 \overline{R} + \eta(m_0 + m_1)$	ηk_0
s^3	α_1	α_2	0
s^2	β_1	ηk_0	
s	γ_1	0	
1	ηk_0		

The stability of the coupled system can be investigated by using the Routh stability criterion, and the corresponding Routh array is listed in Table 1. The terms in Table 1 are:

$$\alpha_1 = \frac{F_i k_c k_d m_0 \overline{R} - \eta L_0 (m_0 + m_1)}{\overline{R}},$$

$$\alpha_2 = \frac{F_i k_c k_d k_0 \overline{R} - \eta L_0 k_0}{\overline{R}},$$

$$\beta_1 = \frac{\eta[\eta L_0 (m_0 + m_1)^2 - \overline{R}(F_i k_c k_d m_0 (m_0 + m_1) - k_0 L_0 m_1^2)]}{\eta L_0 (m_0 + m_1) - F_i k_c k_d m_0 \overline{R}},$$

$$\gamma_1 = \frac{k_0 m_1 \left[\eta L_0 (F_i k_c k_d (m_0 + m_1) - k_0 L_0 m_1) + F_i k_c k_d \overline{R}(k_0 L_0 m_1 - F_i k_c k_d m_0)\right]}{\eta L_0 (m_0 + m_1)^2 - \overline{R}[F_i k_c k_d m_0 (m_0 + m_1) - k_0 L_0 m_1^2]}.$$

The requirement for a stable closed loop is that all the elements in the first column of the Routh array are positive; or alternatively, four conditions must be met:

(1) $\alpha_1 > 0$, this requires:

$$k_c k_d > \frac{\eta L_0 (m_0 + m_1)}{F_i m_0 \overline{R}}; \tag{26}$$

(2) $\beta_1 > 0$, which requires:

$$k_c k_d > \frac{L_0[\overline{R} k_0 m_1^2 + \eta (m_0 + m_1)^2]}{F_i m_0 \overline{R}(m_0 + m_1)}; \tag{27}$$

(3) $\gamma_1 > 0$, which can be satisfied only when:

$$\frac{k_0}{m_0} < \frac{F_i k_c k_d}{m_1 L_0} \frac{F_i k_c k_d m_0 \overline{R} - \eta L_0 (m_0 + m_1)}{F_i k_c k_d m_0 \overline{R} - \eta L_0 m_0} < \frac{F_i k_c k_d}{m_1 L_0}; \tag{28}$$

(4) $\eta k_0 > 0$, which implies

$$F_i k_c k_p - 2 F_z \overline{R} > 0. \tag{29}$$

It can be seen that Eqs. (26), (27) and (29) are the requirements for the control parameters of the coupled levitation system, which are stricter than those for the uncoupled levitation system. Letting $s = j\omega$, gives:

$$\mathrm{Re}[G_0(j\omega)] = \frac{m_1 \eta \omega^2 (F_i k_c k_d - m_1 L_0 \omega^2)}{(\eta - m_1 \overline{R} \omega^2)^2 + \omega^2 (F_i k_c k_d - m_1 L_0 \omega^2)^2}, \tag{30}$$

$$\mathrm{Im}[G_0(j\omega)] = \frac{m_1 \eta \omega (\eta - m_1 \overline{R} \omega^2)}{(\eta - m_1 \overline{R} \omega^2)^2 + \omega^2 (F_i k_c k_d - m_1 L_0 \omega^2)^2}, \tag{31}$$

where $\mathrm{Re}[\cdot]$ and $\mathrm{Im}[\cdot]$ represent the real and imaginary part of the transfer function, respectively. It can be verified that when $\omega = \sqrt{F_i k_c k_d / m_1 L_0}$, $\mathrm{Re}[G_0(j\omega)] = 0$, and $\mathrm{Im}[G_0(j\omega)] < 0$. This implies that $\angle G_0(j\omega) = -\pi/2$ when $\omega = \sqrt{F_i k_c k_d / m_1 L_0}$. Under the assumption that all the control parameters are chosen following the requirements of Eqs. (26), (27) and (29), $G_0(s)$ is a stable and minimum phase system with all its poles in the left half s plane. Referring to Eq. (22), it can be concluded that as ω increases from zero to infinity, the phase of $G_0(j\omega)$ varies within the limits $(-\pi, \pi/2)$. Defining ω_c as the critical frequency of the levitation system at which $\angle G_0(j\omega) = -\pi/2$ allows the following to be written:

$$\omega_c = \sqrt{\frac{F_i k_c k_d}{m_1 L_0}}. \tag{32}$$

For an sdof resonator, it can be easily shown that $k_0/m_0 = \omega_1^2$; therefore, Eq. (28) implies that when the natural frequency of the sdof resonator is higher than the critical frequency of the levitation system, the coupled system becomes unstable and self-excited vibration occurs. This is a sufficient condition for the occurrence of the self-excited vibration, and this conclusion can also be proven using the Nyquist criterion. If $\omega_1 > \omega_c$, according to Eq. (22), it can be verified that

$\angle G_0(j\omega_1) \in (-\pi,-\pi/2)$. Since

$$\angle H(j\omega) = \begin{cases} \dfrac{\pi}{2} & (\omega < \omega_1) \\ -\dfrac{\pi}{2} & (\omega > \omega_1) \end{cases}, \tag{33}$$

then $\angle G_0H(j\omega_1^-) \in (-\pi/2,0)$, and $\angle G_0H(j\omega_1^+) \in (-3\pi/2,-\pi)$.

On the other hand, Eq. (23) implies that $\lim_{\omega\to\omega_1}|H(j\omega)| = \infty$; therefore, $\lim_{\omega\to\omega_1}|G_0H(j\omega)| > 1$, which indicates that the gain of the open loop system is greater than 1 when its phase shift equals $-\pi$. As can be seen, the open loop system, represented by $G_0H(s)$, is minimum phase; thus, it can be concluded that the closed loop system is unstable.

In the discussion above, only the first-order vibration mode of the girder is included. Using the same methodology, it can be shown that higher order vibration modes of the girder may also cause the self-excited vibration problem only if their resonance frequencies are higher than the critical frequency of the levitation system. This is an interesting conclusion since higher order modes of the girder can always be found whose resonance frequencies are higher than the critical frequency of the levitation system. This leads to another conclusion: self-excited vibration will always occur for the electromagnet–girder coupled system. This is true if the damping of the girder is neglected in the girder model. However, in the presence of girder damping, the condition $\lim_{\omega\to\omega_1}|H(j\omega)| = \infty$ does not hold anymore; thus, self-excited vibration may not occur even if the modal resonance frequency is higher than the critical frequency of the levitation system. To demonstrate the effect of damping, suppose that the damping ratio of the nth vibration mode is ζ_n, so the dynamic equation of the girder, Eq. (12), becomes

$$\ddot{y}_n(t) + 2\zeta_n\omega_n\dot{y}(t) + \omega_n^2 y_n(t) = \frac{2F_m}{\rho L}, \quad n = 1,2,\ldots \tag{34}$$

Here, $x_0 = L/2$. For the nth mode, $H(s)$ can be obtained by Eq. (34) using the Laplace transform:

$$H(s) = \frac{sy_n(s)}{F_m(s)} = \frac{s}{m_0(s^2 + 2\zeta_n\omega_n s + \omega_n^2)} \tag{35}$$

from which it can be shown that $|H(j\omega_n)| = (1/2m_0\zeta_n\omega_n)$. This implies that $|H(j\omega_n)|$ is inversely proportional to the modal resonance frequency ω_n. For a real girder, the damping ratio is generally small, so $|H(j\omega_n)|$ is approximately the maximum value of $|H(j\omega)|$ for the nth mode. As ω_n increases, $|H(j\omega_n)|$ becomes smaller and smaller for a constant damping ratio; if the condition $\lim_{\omega\to\omega_n}|GH(j\omega)| > 1$ cannot be guaranteed when $\angle GH(j\omega) = -\pi$, the condition for the occurrence of self-excited vibration will be breached; as a result, the closed loop system becomes stable. Therefore, in practice, the self-excited vibration problem is mainly caused by the lower vibration modes of the girder. Since in most cases the self-excited vibration is caused by the fundamental vibration mode of the girder, the current analysis is directed at suppressing the self-excited vibration of the fundamental vibration mode.

3. Feasibility and stability discussion of applying a TMD to the coupled system

In the previous section, it has been shown that when the natural frequency of the sdof resonator is higher than the critical frequency of the magnetic levitation system, self-excited vibration may occur. This suggests that if the critical frequency of the levitation system can be increased so that the natural frequency of the sdof resonator is lower than the critical frequency of the levitation system, the coupled system will become stable. However, the selection of the control parameters is confined by Eqs. (26), (27) and (29); thus, it is not feasible to increase the critical frequency of the levitation system by adjusting the control parameters only. Since the TMD has been widely applied in the vibration reduction of structures such as tall buildings and bridges, the feasibility of applying a TMD to a maglev girder to suppress the self-excited vibration will be explored here. A schematic of the scheme is shown in Fig. 3. For the purpose of the analysis, it is initially assumed that the TMD is mounted at the same location as the electromagnet.

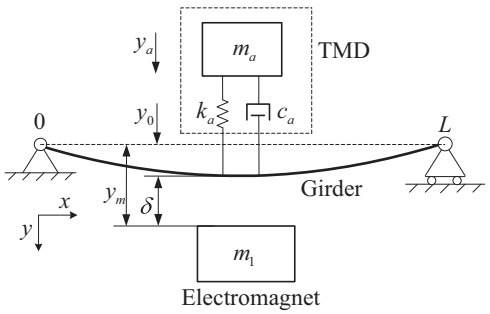

Fig. 3. Schematic of applying a TMD to the maglev girder.

The dynamic equation of the TMD is

$$m_a\ddot{y}_a + c_a(\dot{y}_a - \dot{y}_0) + k_a(y_{a0} + y_a - y_0) = m_a g, \tag{36}$$

where y_{a0} is the static displacement of the spring caused by the gravitational force associated with m_a, and $y_{a0} = m_a g/k_a$. Let F_a denote the force of the TMD acting on the girder, then $F_a = -m_a\ddot{y}_a$, and the transfer function of the TMD can be written in the following form:

$$G_1(s) = \frac{F_a(s)}{sy_0(s)} = \frac{m_a s(c_a s + k_a)}{m_a s^2 + c_a s + k_a}. \tag{37}$$

Taking the dynamics of the TMD into account, the block diagram of the closed loop system is shown in Fig. 4, in which F_0 is the resultant force acting on the girder.

Now let $G(s)$ denote the transfer function of the forward path, then

$$G(s) = G_0(s) + G_1(s). \tag{38}$$

The feedback path, $H(s)$, is positive real since $\mathrm{Re}[H(j\omega)] = 0$, $\forall\omega > 0$. Therefore, if $G(s)$ is strictly positive real, that is, $\mathrm{Re}[G(j\omega)] > 0$, $\forall\omega > 0$ (which is also strictly passive for a linear, time invariant system), then the closed loop system will be asymptotically stable since the negative feedback connection of any passive and strictly passive system is asymptotically stable [16,17]. From Eq. (37), the real part of $G_1(j\omega)$ can be obtained as

$$\mathrm{Re}[G_1(j\omega)] = \frac{m_a^2 c_a \omega^4}{(k_a - m_a\omega^2)^2 + c_a^2\omega^2}. \tag{39}$$

Combined with Eq. (30), the TMD parameters should satisfy the following inequality if $G(s)$ is strictly positive real:

$$\frac{m_1\eta\omega^2(F_i k_c k_d - m_1 L_0\omega^2)}{(\eta - m_1\bar{R}\omega^2)^2 + \omega^2(F_i k_c k_d - m_1 L_0\omega^2)^2} + \frac{m_a^2 c_a\omega^4}{(k_a - m_a\omega^2)^2 + c_a^2\omega^2} > 0, \quad \forall\omega > 0. \tag{40}$$

This is the only requirement for the TMD to stabilize the coupled system. Since there are three unknown parameters to determine, the result is not unique. Given the parameters of the electromagnet and the girder, as well as the control parameters, a group of TMD parameters can be chosen by trial and error before the system comes online. However, for an adaptive levitation control system, the control parameters may be updated during operation, which requires the TMD parameters to be updated according to the real time control parameters when the self-excited vibration occurs. Thus, a procedure to calculate the TMD parameters is described in the paragraphs to follow.

Differentiating Eq. (39) with respect to ω, and letting the result equal zero gives the center frequency of the TMD as

$$\omega_a = \sqrt{\frac{k_a^2}{k_a m_a - c_a^2}}, \tag{41}$$

which is approximately equal to $\sqrt{k_a/m_a}$ if the damping ratio of the TMD is sufficiently small. The value of $\mathrm{Re}[G_1(j\omega)]$ at ω_a is

$$P_a = \frac{k_a m_a}{2c_a}. \tag{42}$$

The bandwidth is an important parameter for the TMD. Here, the bandwidth is defined as the frequency band within which $\mathrm{Re}[G_1(j\omega)]$ is equal or greater than 0.5 P_a. It can be deduced from Eq. (39) that the frequencies corresponding to 0.5 P_a are:

$$\omega_{b1} = k_a\sqrt{\frac{2k_a m_a - c_a^2 - c_a\sqrt{4k_a m_a - c_a^2}}{c_a^4 - 4c_a^2 k_a m_a + 2k_a^2 m_a^2}} \tag{43}$$

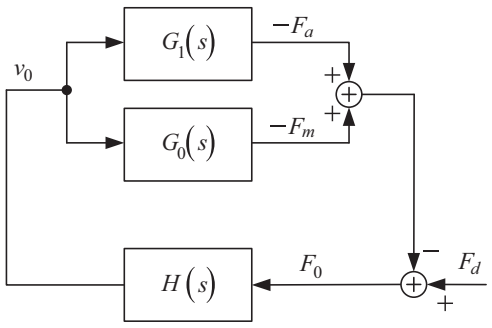

Fig. 4. Block diagram of the closed loop system with a TMD.

and

$$\omega_{b2} = k_a \sqrt{\frac{2k_a m_a - c_a^2 + c_a\sqrt{4k_a m_a - c_a^2}}{c_a^4 - 4c_a^2 k_a m_a + 2k_a^2 m_a^2}}. \tag{44}$$

Therefore, the bandwidth of the TMD is

$$BW_a = \omega_{b2} - \omega_{b1}. \tag{45}$$

When the damping ratio of the TMD is small, the result can be simply approximated as

$$BW_a \approx \frac{c_a}{m_a}. \tag{46}$$

Extensive simulations indicate that the TMD parameters can be determined by the following procedure:

(1) Determine the central frequency of the TMD, ω_a. This can be done by choosing ω_a to be the frequency corresponding to the minimum value of $\mathrm{Re}[G_0(j\omega)]$. Using Eq. (30), ω_a can be obtained. As this is a difficult task, an empirical formula can be employed to obtain an approximate solution:

$$\omega_a = -52.188 - 8.8709 \times 10^{-3} k_p + 2.7532 k_d - 1.4121 \times 10^{-2} k_d^2 + 2.7449 k_c - 0.0079424 k_c^2. \tag{47}$$

(2) Set $P_a = 4\mathrm{Re}[G_0(j\omega_a)]$, and $BW_a = 1.3(\omega_a - \omega_c)$.
Then the three parameters of the TMD can be calculated using the following equations:

$$m_a = \frac{2BW_a P_a}{\omega_a^2}, \tag{48}$$

$$k_a = \omega_a^2 m_a, \tag{49}$$

$$c_a = \frac{2BW_a^2 P_a}{\omega_a^2}. \tag{50}$$

For a full-scale, low-speed, maglev system, the parameters characterizing the electromagnet and the control parameters are listed in Table 2. Using the TMD design procedure listed above, the corresponding set of TMD parameters are found to be: m_a=89.42 kg, $k_a = 1.047 \times 10^6$ N m^{-1}, and $c_a = 2554$ N s m^{-1}. For a SISO, linear, time-invariant system, the condition for $G(s)$ to be strictly positive real is equivalent to $\angle G(j\omega) \in (-\pi/2, \pi/2)$, $\forall \omega > 0$. Fig. 5 shows the amplitude and phase response of $G(j\omega)$ with the compensation of $G_1(s)$, from which it can be seen that with the chosen TMD parameters, the transfer function of the forward path $G(s)$ is strictly positive real; therefore, the corresponding closed loop system is stable.

The stability of the closed loop system can be validated by numerical simulation. Assuming that the equivalent mass and stiffness of the girder, which has been modeled as an sdof resonator, are m_0=8000 kg, and $k_0 = 1.0 \times 10^8$ N/m, respectively, then the natural frequency of the sdof resonator is 17.79 Hz. The critical frequency of the levitation system can be calculated by Eq. (32), which is 13.44 Hz, and this is lower than the natural frequency of the sdof resonator. Accordingly, the coupled system, as shown in Fig. 2, is unstable and self-excited vibration will occur. Fig. 6(a) shows the response of the levitation gap, from which it is confirmed that the closed loop system is unstable. In contrast with Fig. 6(a), Fig. 6(b) shows the response of the levitation gap when the designed TMD is mounted to the girder at the same location as that of the electromagnet. It can be seen that the resulting closed loop system, which corresponds to Fig. 4, is asymptotically stable. The simulation conducted here is based on the nonlinear dynamic model; in other words, the dynamic model of the levitation system used in the simulation is Eqs. (3)–(5), (7), (8), and (19), rather than the linearized model described by Eq. (21). The nonlinear simulation shows good agreement with the analysis undertaken using the linearized model.

Table 2
Parameters of the levitation system.

Variable	Value	Unit
m_1	510	kg
z_0	0.008	m
μ_0	$4\pi \times 10^{-7}$	H m^{-1}
A	0.02352	m^2
N	320	–
g	9.81	m s^{-2}
R	0.56	Ohm
k_p	4400	–
k_d	50	–
k_c	40	–

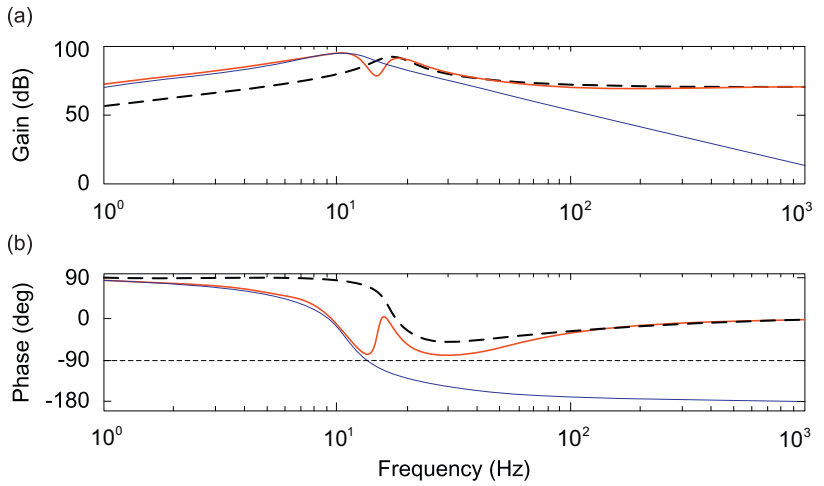

Fig. 5. Frequency response of $G(s)$ with compensation of $G_1(s)$: (a) magnitude–frequency response curves and (b) phase–frequency response curves. (—) $G_0(s)$, (- - -) $G_1(s)$, (–) $G_0(s) + G_1(s)$.

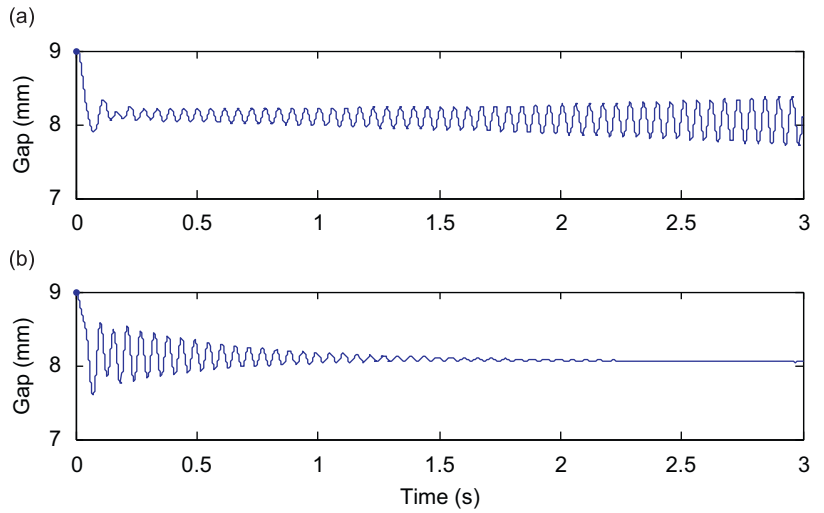

Fig. 6. Closed loop response of the levitation gap: (a) levitation gap response without TMD and (b) levitation gap response with TMD mounted to the girder.

As shown by the inequality of Eq. (40), the selection of the TMD parameters is independent of the girder parameters, provided that the TMD and the electromagnets are at the same location on the girder. Unfortunately, the requirement that the TMD and the electromagnet are at the same location is hard to meet, since it is uncertain where the maglev train stops. To overcome this problem, optimization process may be conducted to decide the best location where the TMD should be mounted when the electromagnet is moving along the girder. However, this problem may also be solved by using the virtual TMD scheme, which will be discussed in the next section.

4. Realization of the virtual TMD

The electromagnets in a maglev vehicle are excellent actuators that are capable of providing sufficiently large forces acting on the girder to emulate the force of a TMD. However, several practical problems need to be taken into account when designing the virtual TMD. First, the optimal structure of the virtual TMD must be determined; second, a means to estimate the movement of a real TMD needs to be devised; and third, the problem caused by the actuation delay needs to be solved.

4.1. Structure of the virtual TMD

Observing the third equation in Eq. (21), it can be shown that the electromagnetic force is approximately proportional to the current through the electromagnet around the equilibrium point. Hence, once the force, $\hat{F}_a$, that the TMD applies to the girder is estimated, an additional current (which is referred to as i_{ea}) with an amplitude of $\hat{F}_a/2F_i$ is required for the electromagnets to generate the desired TMD force. Consequently, Eq. (8) becomes:

$$u(t) = k_c[i_e(t) + \hat{F}_a(t)/2F_i - i(t)]. \tag{51}$$

If the closed loop system is asymptotically stable, the steady-state current will be approximately the sum of i_e and i_{ea}. Eq. (51) also reveals that the capacity of a virtual TMD is constrained by the maximum output force of the electromagnet. For an EMS maglev system, the electromagnet can only produce an attraction force. In a normal case, a constant attraction force F_e, which corresponds to the load of the electromagnet, acts on the girder. Therefore, around the equilibrium point, the maximum negative force that an electromagnet can provide is $-F_e$, which is the case when i=0. At this point, the capacity of a single VTMD is mostly constrained by the load of the electromagnet. However, this is only the capacity for a single levitation unit, and this capacity may be greatly extended when multiple levitation units are taken into account.

The state estimation of the TMD relies on the movement of the girder, which, however, is not easy to measure since it is hard to find a sensor that could measure the movement of the elevated girder in the inertial space. Therefore, the real time movement estimation of the girder at the location of the electromagnets is essential to enable successful use of the virtual TMD. In a real maglev vehicle, two states, including the levitation gap, δ, which can be measured by an eddy current gap sensor, and the acceleration of the electromagnet, a_1, which can be measured by an accelerometer, are available. From Fig.1, it can be seen that $y_0 = y_m - \delta$. Using the accelerometer and the eddy current gap sensor as inputs of the state estimator, estimates of the displacement and velocity of the girder, which are represented as $\hat{y}_0$ and $\hat{\dot{y}}_0$, respectively, can be obtained by using the following estimator:

$$\begin{cases} \dot{x}_1 = -\lambda_1 x_1 + a_m \\ \dot{x}_2 = -\lambda_1 x_1 + a_m \\ \dot{x}_3 = x_2 \\ \dot{x}_4 = -\lambda_2 x_4 + \delta \\ \hat{y}_0 = x_3 - \lambda_2 x_4 \\ \hat{\dot{y}}_0 = x_2 + \lambda_2 x_4 - \delta \end{cases}. \tag{52}$$

The estimator, which can be regarded as a filter, is always stable provided that λ_1 and λ_2 are both positive. The values of λ_1 and λ_2 also determine the bandwidth of the estimator. According to the natural frequency, ω_1, of the sdof resonator the parameters can be chosen as $\lambda_1 \le 0.1\omega_1$ and $\lambda_2 \ge 20\omega_1$. This estimator is capable of estimating the movement of the girder whilst filtering out the DC bias mixed within the measured acceleration signal.

The block diagram of the closed loop system with estimator is shown in Fig. 7, in which the block EM represents the electrodynamic Eqs. (3) and (4), GDR is the dynamic model of the girder, and EST is the state estimator which is described by Eq. (52).

In some previous research which concerns the study of the virtual TMD, the dynamics of the actuator has been neglected [9–11]. This may have been because the time delay caused by the actuator is sufficiently small that it has little effect on the stability of the closed loop system. However, in the low speed EMS maglev system considered here, the inductance of a single electromagnet reaches 0.1 H (the inductance is highly related to the air gap between the electromagnet and the steel track; here the inductance is estimated around the desired levitation gap, which is 8 mm); therefore, compared with the period of the free vibration of the girder, the electromagnetic force delay cannot be neglected, and a procedure must be undertaken to compensate for the actuation time delay.

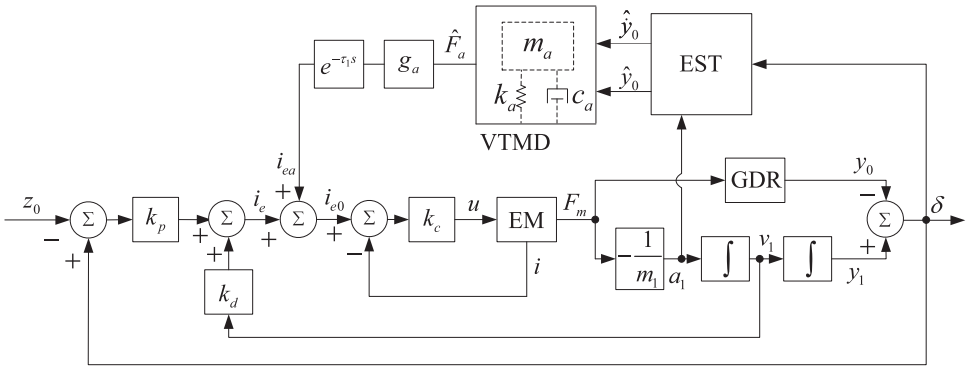

Fig. 7. Block diagram of the levitation system with the virtual TMD.

In previous work where the actuation delay has been taken into account, several strategies have been applied to compensate the stability of the system [13–15], as discussed in the introduction. However, none of these are applicable to the maglev system. Since the self-excited vibration is approximately periodic, the phase of the feedback signal can be adjusted by intentionally delaying the feedback signal for a certain amount of time, τ_1. If the actuation time delay, τ_0, together with τ_1, equals the period of the vibration, then the additional force generated by the electromagnet should be in phase with the estimated TMD force $\hat{F}_a$, and the effect of the actuation delay may be neutralized. This idea is sketched in Fig. 7, in which $e^{-\tau_1 s}$ is the intentionally introduced time delay that is used for time delay compensation, and g_a is the gain of the feedback signal.

Taking the time delay in the virtual TMD feedback path into account, the simplified closed loop system is shown in Fig. 8, in which β is the force gain, and $\beta=g_a/2F_i$. Note that the time delay, τ, in Fig. 8 includes both the actuation delay and the intentionally introduced time delay. It shall be shown that there exist a series of time delays $\{\tau_n\}$ $(n=1, 2,\dots)$ such that the closed loop system is stable. To simplify the proof, it is first supposed that $\beta=1$. This is the case when the force of the virtual TMD is fully fed back to the controller without amplification. Suppose that the original coupled system is unstable. In this case, the natural frequency of the sdof resonator is higher than the critical frequency of the levitation system; namely $\omega_1 > \omega_c$. Then:

$$\angle[G_0(j\omega_1)] \in \left(-\pi, -\frac{\pi}{2}\right). \tag{53}$$

Since the designed TMD stabilizes the closed loop system, this suggests that

$$\angle[G_0(j\omega_1)+G_1(j\omega_1)] \in \left(-\frac{\pi}{2}, \frac{\pi}{2}\right). \tag{54}$$

On the other hand:

$$\angle[G_1(s)e^{-\tau s}]\big|_{s=j\omega_1} = \angle[G_1(j\omega_1)] - \tau\omega_1 \tag{55}$$

and

$$\left|G_1(s)e^{-\tau s}\right|\big|_{s=j\omega_1} = \left|G_1(j\omega_1)\right|, \tag{56}$$

therefore, if $\tau\omega_1 = 2n\pi$, or $\tau = 2n\pi/\omega_1$, then

$$G_1(s)e^{-\tau s}\big|_{s=j\omega_1} = G_1(j\omega_1) \tag{57}$$

and

$$\angle[G_0(s)+G_1(s)e^{-\tau s}]\Big|_{s=j\omega_1} = \angle[G_0(s)+G_1(s)]\Big|_{s=j\omega_1} \in \left(-\frac{\pi}{2}, \frac{\pi}{2}\right). \tag{58}$$

In Section 2, it was shown that $\angle[G(j\omega_1)] \in (-\pi, -(\pi/2))$ is a sufficient condition for the occurrence of the self-excited vibration, where $G(s)$ is the feedforward path in Fig. 8. Therefore, Eq. (58) is a necessary condition for the stability of the closed loop system, although it does not guarantee that the closed loop system will be stable. However, it demonstrates that the closed loop system may be stabilized by adjusting the time delay of the TMD feedback path such that the total actuation time delay matches one or more periods of the vibration. When the gain β is taken into account, the stability of the closed loop system will be much more complex. However, it provides a strategy to extend the stability region of the system, which will be discussed using the root locus method in the following section.

4.2. Stability analysis of the virtual TMD in the magnetic levitation system

From Fig. 8, the open loop transfer function can be written as

$$GH(s) = [G_0(s)+\beta G_1(s)e^{-\tau s}]H(s). \tag{59}$$

Substituting Eqs. (22), (23) and (37) into Eq. (59), yields

$$GH(s) = \frac{\Delta_1(s)\eta m_1 s^2 + \beta\Delta_0(s)m_a s^2(m_a s + k_a)e^{-\tau s}}{\Delta_0(s)\Delta_1(s)\Delta_a(s)}, \tag{60}$$

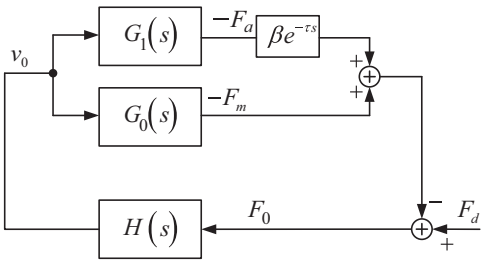

Fig. 8. Block diagram of the closed loop system when the time delay is taken into account.

where $\Delta_0(s)$, $\Delta_1(s)$, and $\Delta_a(s)$ are the denominators of $G_0(s)$, $G_1(s)$ and $G_a(s)$, respectively. Therefore, the characteristic polynomial of the closed loop system is

$$\Delta(s) = 1 + GH(s) = 1 + \frac{\Delta_1(s)\eta m_1 s^2 + \beta\Delta_0(s) m_a s^2 (m_a s + k_a) e^{-\tau s}}{\Delta_0(s)\Delta_1(s)\Delta_a(s)}. \tag{61}$$

If s is a root of the closed loop system, then $\Delta(s)=0$. This is a transcendental equation, and can be rearranged as

$$1 + \frac{\beta\Delta_0(s) m_a s^2 (m_a s + k_a) e^{-\tau s}}{\Delta_0(s)\Delta_1(s)\Delta_a(s) + \Delta_1(s)\eta m_1 s^2} = 0. \tag{62}$$

If $s=\sigma+j\omega$ is a root of the closed loop system, the angle condition gives

$$\angle[\Delta_0(s) m_a s^2 (m_a s + k_a)] - \angle[\Delta_0(s)\Delta_1(s)\Delta_a(s) + \Delta_1(s)\eta m_1 s^2] = (2l-1)\pi + \tau\omega, \quad l = 1,2,\ldots \tag{63}$$

and the magnitude requirement is

$$\left| \frac{\beta\Delta_0(s) m_a s^2 (m_a s + k_a) e^{-\tau s}}{\Delta_0(s)\Delta_1(s)\Delta_a(s) + \Delta_1(s)\eta m_1 s^2} \right| = 1. \tag{64}$$

If $\tau > 0$, there will be an infinite number of roots for Eq. (63). For comparison, the root locus of the closed loop system when the time delay $\tau=0$ is shown in Fig. 9.

From Fig. 9, it can be seen that the closed loop system is stable when $\beta=1$. This is equivalent to the case when a real TMD is mounted to the girder, and the stability of this case has been proven in the previous section. From Fig. 9(b), it can also be seen that without the TMD (when $\beta=0$), the closed loop system is unstable, and that $\beta=0.237$ is the minimum gain that stabilizes the closed loop system.

When the time delay is nonzero, the root locus of the system will be quite different. As mentioned earlier, there are an infinite number of solutions that satisfy the phase condition of Eq. (63); therefore, the most significant difference of the root loci with feedback time delay is that the number of root loci is infinite, and most of them will cross the imaginary axis and reach the right half-plane as the gain increases. Fig. 10(a) shows the root locus of the system when $\tau=0.01$ s, from which it can be seen that many additional root loci appear in the chart, and they tend to cross the imaginary axis as the gain β increases. The root loci are calculated using the Newton–Raphson iteration method and are validated by the gradient method [18]. Fig. 10(b) shows the detail of the region around the origin. The labels r_1–r_3 in the figure stand for the root loci departing from p_1 to p_3, and r_1' to r_3' are the conjugates of r_1–r_3. Similarly, l_1, l_2 and l_1', l_2' in Fig. 10(a) represent the additional root loci introduced by the time delay. It can be seen that r_1 and r_1' are the dominating loci when the time delay is 0.01 s. They first cross into the left half-complex plane, and then turn to the right hand side as the gain β increases. This indicates that there exists a stable gain range within which the closed loop system is stable.

However, r_1 and r_1' are not always the dominating loci as the time delay τ increases. The stable gain boundaries for r_1–r_3 and l_1–l_3 are shown in Fig. 11(a), and the details around the τ-axis are shown in Fig. 11(b). The other additional branches, l_4, l_5…, are not plotted in the figure. It can be seen that only r_1 has a lower gain boundary, but the upper gain boundary is dominated by some other branches. From Fig. 11(b), it can be seen that the lower gain boundary and the upper gain boundaries form a series of isolated triangles (the hatched areas in the figure); therefore, if τ and β are chosen within these triangles, the coupled system will be stabilized.

It can also be seen that the stable regions appear periodically as the time delay increases, and that the period of these triangles, τ_c, is 0.056 s, which equals the period of the vibration, $2\pi/\omega_1$ (in the simulation, the natural frequency of the sdof

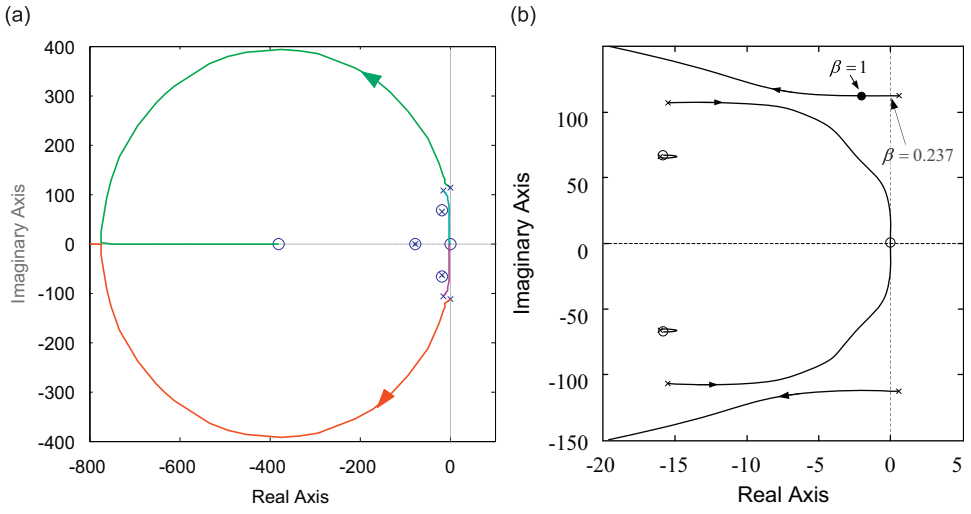

Fig. 9. Root locus of the system when the time delay is neglected: (a) the overall root loci and (b) the local details of the root loci around the origin.

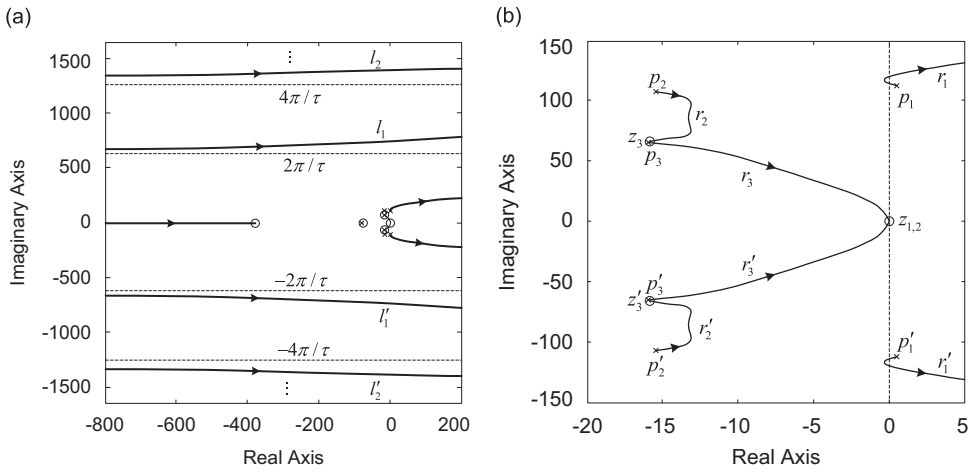

Fig.10. Root locus of the system when the time delay is 0.01 s: (a) the overall root loci and (b) the local structure of the root loci around the origin.

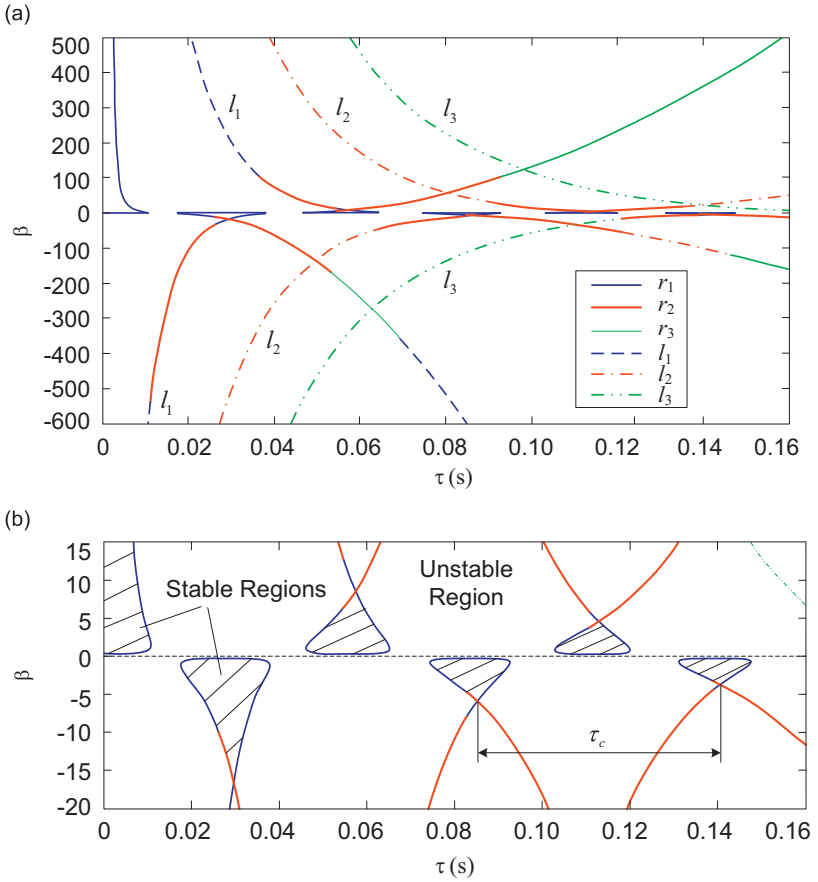

Fig. 11. Stable regions for the feedback gain in the presence of actuation time delay: (a) the overall view of the gain boundaries; and (b) detailed view of the stable regions.

system, ω_1, is 111.8 rad/s, thus $2\pi/\omega_1$=0.056 s). This agrees well with our assumption that there exists a series of time delays $\{\tau_n\}$ (n=1, 2…) such that the closed loop system is stable.

However, as the time delay increases, the height of the triangles becomes lower and lower, which indicates that the allowed gain range decreases. Therefore, the most applicable time delay that can be used in the feedback path should be as

small as possible. It has been shown that the period separating the triangles is

$$\tau_c = \frac{2\pi}{\omega_1}, \tag{65}$$

which is the same as the period of the vibration. Suppose that the total time delay caused by the electromagnets is τ_0, then to stabilize the system, an additional time delay, τ_1, can be intentionally introduced in the TMD feedback path such that $\tau_0+\tau_1$ lies in one of the triangles shown in Fig. 11(b). To achieve this, the most suitable time delay τ_1 can be chosen as

$$\tau_1 = (n+1)\frac{\tau_c}{2} - \tau_0, \quad n = \mathrm{Int}\left(\frac{2\tau_0}{\tau_c}\right), \tag{66}$$

where $\mathrm{Int}(\cdot)$ is a function that returns the integer part of a specified value. The integer number n indicates which triangle τ_0 lies in, and Eq. (66) guarantees that $\tau_0+\tau_1$ corresponds to the center line of a triangle. This gives a maximum stable gain range for β. On the other hand, from Fig. 11(b), it can be seen that setting β to be around ± 1 achieves the widest stable range for the time delay; thus β can be chosen as

$$\beta = (-1)^{n+1}. \tag{67}$$

Eqs. (65)–(67) guarantee that the selected time delay τ_1 is optimal, and the equations also make it possible for the process to be implemented in a computerized controller, given that τ_0 and τ_c (or ω_1) can be estimated.

4.3. Procedure of designing a virtual TMD

As discussed above, once the period of the vibration, τ_c, and the time delay of the electromagnet, τ_0, are known, the optimal additional time delay τ_1, and the TMD feedback gain, β, can be determined using Eqs. (66) and (67). For τ_c, a knowledge base can be established if the frequency of the self-excited vibration on each girder along the maglev route can be measured *a priori*. With the assistance of the absolute position detection system in a maglev vehicle, the position of the vehicle can be determined; thus the vibration frequency can be retrieved from the knowledge base, and τ_c can be obtained using Eq. (65). Alternatively, if the information of the vibration frequency along the route is not available, it can be estimated online by several different methods that are normally used in spectral estimation problems, such as FFT, and auto-correlation analysis. A simple zero crossing detector was applied by Elmali et al. [17], to calculate the vibration frequency of the primary structure in the delayed resonator scheme. This method, although straightforward in implementation, may be inaccurate when the signal–noise ratio is poor. Additionally, adaptive notch filters may be a good choice for the frequency estimation [19].

The actuation time delay, τ_0, is not constant, but is variable and is related to the frequency of the self-excited vibration. Therefore, a straightforward method of estimating τ_0 is to establish a table that stores τ_0 corresponding to different vibration frequencies. This can be achieved by introducing a sinusoidal disturbance into the desired control current, i_e, and measuring the phase shift between the input disturbance and the acceleration of the electromagnets. For example, suppose that the disturbance can be described as $d(t)=A_0\sin(2\pi f_d t)$, where f_d is the frequency of the disturbance, A_0 is the amplitude of the disturbance, and the acceleration response of the electromagnets is $a_1(t)$, which is approximately sinusoidal when A_0 is small. Suppose that the phase lag from $d(t)$ to $a_1(t)$ is φ, then the actuation time delay can be obtained as: $\tau_0=\varphi/(2\pi f_d)$. Given a series of disturbances at different frequencies, a series of time delays can be obtained, and a table of τ_0 vs. f_d can thus be established. This work can be done offline. Once τ_c or the frequency of the self-excited vibration has been obtained, τ_0 can be retrieved from the table. Another method is to compute the cross correlation of $i_e(t)$ and $a_1(t)$, and to calculate τ_0 according to the maximum peak of the correlation. This method is applicable when the self-excited vibration is occurring.

In summary, the design procedure of the virtual TMD can be generalized as follows:

(1) Calculate the parameters of a real TMD that can render the levitation system to be positive real. The parameters can be calculated using Eqs. (48)–(50).
(2) Estimate τ_c, which can be calculated according to the frequency of the self-excited vibration, which, in turn, can be obtained through real time estimation or by prior knowledge using the position detection system.
(3) Estimate the actuation time delay, τ_0, which can be done by looking it up from a τ_0 vs. f_d table. Alternatively, it can be estimated online by calculating the cross correlation of $i_e(t)$ and $a_1(t)$.
(4) Use Eqs. (66) and (67) to determine the optimal additional time delay τ_1 and gain β for the TMD feedback path.

As the vehicle may stop at any location along the maglev route, the values of τ_c and τ_0 should be updated from time to time, and the optimal time delay τ_1 and gain β should be updated accordingly. This can be done by repeating steps (2)–(4). It should be noted that the proposed scheme is directed at solving the stationary vehicle–girder self-excited vibration; therefore, when the vehicle is running at a relatively high speed, this algorithm will be switched off since in such a case, the vehicle will pass through a girder within a short time, and the self-excited vibration is unlikely to occur.

5. Numerical simulation

To verify the effectiveness of the proposed virtual TMD scheme, a numerical simulation has been undertaken. The parameters of the magnetic levitation system are chosen from Table 2, and the TMD parameters are chosen to be the same as in Section 3, which are: m_a=89.42 kg, $k_a = 1.047 \times 10^6$ N m^{-1}, and $c_a = 2554$ N s m^{-1}. Since only the fundamental mode of the girder is of concern, as discussed in Section 2, the model of the girder can be simplified as an sdof system. Here, it is assumed that the equivalent parameters of the sdof system are: m_0=8000 kg, $k_0 = 1.0 \times 10^8$ N m^{-1}, and c_0=0 N s m^{-1}. The parameters of the state estimator are chosen as λ_1=5, λ_2=2000.

According to the design procedure outlined at the end of the previous section, first the resonance frequency of the girder is calculated, which is $\omega_1 = \sqrt{k_0/m_0} = 111.8$ rad s^{-1}, thus $\tau_c = 2\pi/\omega_1 = 0.0562$ s. As mentioned earlier, either a look up table or real time estimation can be applied to get the actuator time delay. Here, a real time estimation method is applied using the cross correlation of $i_e(t)$ and $-a_1(t)$. Here, the negative sign in front of $a_1(t)$ denotes that the direction of the virtual TMD force acting on the girder, $\hat{F}_a(t)$, is opposite to $a_1(t)$. To reduce the computational effort, three circular queues are applied to store the historical data of $i_e(t)$, $-a_1(t)$, and $\hat{F}_a(t)$, respectively. The length of a circular queue is such that it is able to store up to 0.6 s of the latest data. The result of the correlation is stored in a buffer S, and is computed using the following equation:

$$S(k) = -\sum_{n=1}^{N} i_e(nT)a_1[(n+k)T], \quad k = 0,1,\ldots,K, \tag{68}$$

where N is the total number of data samples in a single queue, T is the sampling period, and KT is the maximum time shift that is expected. In Eq. (68), it should be noted that $a_1[(n+k)T] = a_1[(n+k-N)T]$, if $n+k > N$. If the location of the first peak that appears in S is at k_0, then the time delay from $i_e(t)$ to $a_1(t)$ is k_0T. Using Eqs. (66) and (67), the optimal time delay and gain can then be calculated.

Fig. 12(a) shows the simulation result for the levitation gap. The virtual TMD and the time delay estimator have come into operation once the simulation begins. However, for comparison, within the first 1.5 s, the feedback gain β is intentionally set equal to zero, which is the case when the virtual TMD is deactivated. The stability of the coupled system without the TMD has been discussed in Section 3, in which it was concluded that self-excited vibration will occur when the natural frequency of the sdof system is higher than the critical frequency of the levitation system. The simulation confirms this conclusion, and it can be seen that without vibration control algorithm, the amplitude of the vibration grows with time and it can lead to a levitation failure.

In the simulation, it is found that the first peak of the cross correlation appears at around 5.2 ms; therefore, τ_0=5.2 ms. The first trough of the cross correlation appears at 32.4 ms, thus the period of the vibration is $2 \times (32.4–5.2)$=54.4 ms, namely, τ_c=54.4 ms. According to Eq. (66), it can be found that n=0 and τ_1=22 ms. Using Eq. (67), the gain of the TMD feedback path can be determined as β=–1.

At the time mark of 1.5 s, the virtual TMD is activated by replacing the feedback gain β with the value calculated by Eq. (67). It can be seen that the amplitude of the vibration attenuates quickly. Fig. 12(b) shows the estimated optimal time

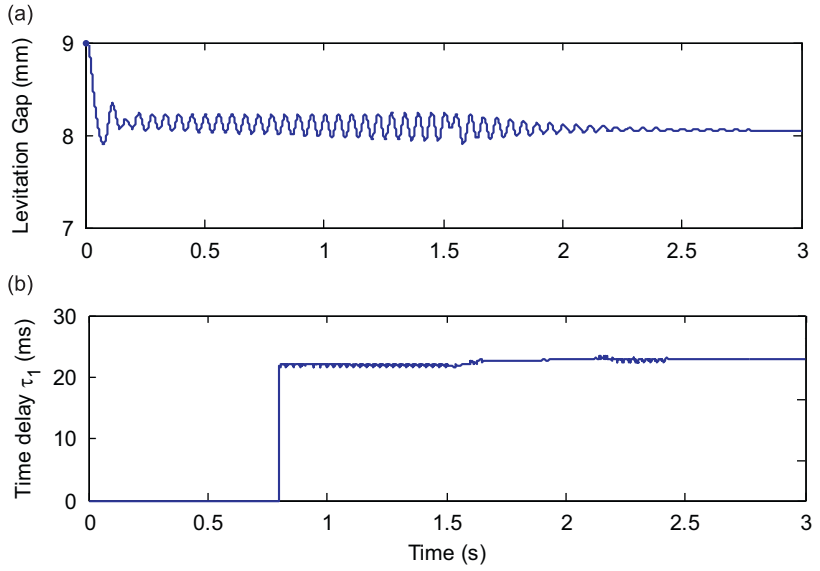

Fig. 12. Simulation result. The feedback gain of the virtual TMD, β, is intentionally set to be zero within the first 1.5 s, and is restored to –1 after 1.5 s: (a) the levitation gap; (b) the estimated optimal time delay for the TMD feedback path. The estimation commences at 0.8 s, after the circular queues are fully filled.

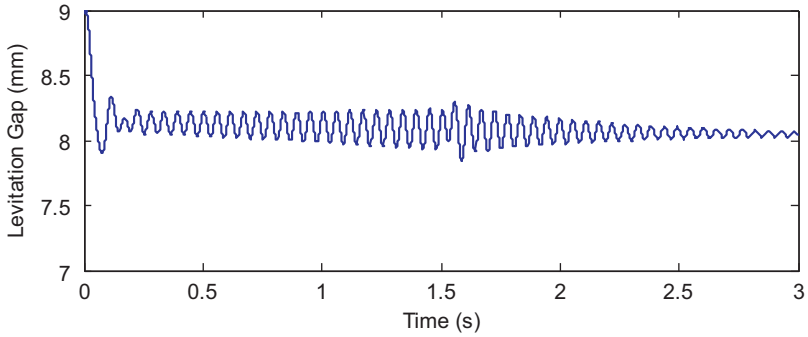

Fig. 13. Response of the levitation gap when additional time delay, τ_1, is set to zero throughout the simulation. The feedback gain of the virtual TMD, β, is set to be zero within the first 1.5 s, and is restored to be +1 after 1.5 s.

delay τ_1. Since the lengths of the circular queues are 0.6 s, at least 0.6 s is required to fill up the queues with measured data. In addition, taking the transient response time of the levitation system into account, it is appropriate to activate the estimation after 0.8 s. It can be seen that before the activation of the virtual TMD, the optimal time delay τ_1 estimated by Eq. (66) is around 22 ms, and tiny ripples can be found in the τ_1 vs. time curve. This is mainly caused by the limited precision of the cross correlation calculation. As the amplitude of the vibration dies away, the precision of the cross correlation will become poorer and poorer, which may result in an incorrect estimation result. To avoid this problem, a threshold, *cc*, is applied to the cross correlation, and updates of τ_0, τ_1, and β are only calculated and used when the peak value of the cross correlation exceeds *cc*.

In the simulation, the cross correlation of $i_e(t)$ and $-a_1(t)$ shows that the time delay between them is about 5.2 ms. Referring to Fig. 11(b), it can be found that the actuation time delay corresponds to the first positive triangle, which suggests that without additional time delay in the TMD feedback path, the system should be stable if the gain of the TMD is +1. This can be verified in the simulation.

Fig. 13 shows the response of the levitation gap when τ_1 is fixed to be zero, and β is set equal to +1. In this case, no additional time delay is required, and the feedback is quite simple. It can be seen that under such a condition, the closed loop system can also be stabilized, although the attenuation of the vibration is slower than that shown in Fig. 12(a). However, as the resonance frequency of the girder changes, the actuation time delay also changes, and setting $\tau=0$ cannot guarantee that the actuation time delay always lies in one of the stable regions. In this case, an additional time delay is required to keep the total time delay within one of the triangles shown in Fig. 11.

In the discussion above, only the first-order vibration mode of the girder was considered. In fact, as long as the self-excited vibration occurs at a single frequency, the scheme discussed above is still applicable, regardless of the order of the unstable vibration mode. Fortunately, in practice, it has been found that the self-excited vibration that occurs in a low-speed maglev system is mostly at a single frequency. However, when more than one unstable vibration modes of the girder are taken into account, the behavior of the algorithm will become quite complicated, and two results are likely to be obtained, depending on the techniques that are used to estimate the frequency of the girder. First, the algorithm suppresses only one unstable mode, and the other unstable modes cannot be suppressed. This is the case when the resonance frequency of the girder is retrieved from a knowledge base. Second, the algorithm may get confused and be unable to determine the period of the vibration, thus failing to suppress either one of the unstable vibration modes. This is the case when the real time estimation method is used. To suppress the coupled vibration caused by more than one unstable vibration mode, multiple virtual TMDs and multiple frequency estimation methods are required, and this is a subject that will be addressed in future work.

6. Conclusions

The coupled model of an EMS magnetic levitation system and a flexible girder has been analyzed and modal analysis shows that the girder can be replaced by a series of sdof mass–spring resonators. Higher order vibration modes of the girder have been neglected in the analysis since their equivalent mechanical impedances increase rapidly with the index number of the order, and a single sdof resonator is employed as representative of a specified vibration mode of the girder in the analysis. Using the Nyquist criterion, it is found that when the damping of the girder is neglected, self-excited vibration may occur if the resonance frequency of the sdof system is higher than the critical frequency of the levitation system. However, in the presence of girder damping, higher order vibration modes of the girder are unlikely to cause the self-excited vibration.

The stability resulting from applying a TMD to the coupled system has been discussed, which shows that the TMD can suppress to a large extent the self-excited vibration, if the parameters of the TMD are properly chosen. This conclusion is based on the TMD being mounted to the girder at the same location as the electromagnet. This constraint is a handicap for

the application of an actual TMD, but is not a problem for the application of the virtual TMD system discussed in this paper, since the constraint is always satisfied for this case.

In the presence of actuation time delay caused by the inductance of the electromagnets, the stability of the virtual TMD becomes complex to characterize. To explore the stability, the root locus of the system with a virtual TMD has been examined and it was found that as the actuation time delay increases, there exists a stable gain region corresponding to the time delay lying in some specific ranges. It was found that these stable gain regions have shapes similar to triangles, and that the intervals between the triangles are the same, with the actual interval related to the vibration frequency. This character enables the determination of the optimal time delay in the TMD feedback path if the frequency of the self-excited vibration as well as the time delay of the actuator can be estimated. To achieve this, a scheme for estimating the frequency of the vibration and the actuation time delay was proposed, using the cross correlation between the desired control current and the motion of the electro magnet. A numerical simulation demonstrated the validity of the stability analysis, and also showed that the proposed virtual TMD scheme is capable of suppressing the vehicle–girder self-excited vibration caused by a single unstable vibration mode.

Acknowledgments

The authors gratefully acknowledge financial support provided by National Key Technology R&D Program (No. 2006BAG02B05-04) and the National Nature and Science Foundation of China (No. 60404003).

References

[1] L.G. Yan, Development and application of the maglev transportation system, *IEEE Transactions on Applied Superconductivity* 18 (2) (2008) 92–99.
[2] D.F. Zhou, C.H. Hansen, J. Li, W.S. Chang, Review of coupled vibration problems in EMS maglev vehicles, *International Journal of Acoustics and Vibration* 15 (1) (2010) 10–23.
[3] J.D. Yau, Vibration control of maglev vehicles traveling over a flexible guideway, *Journal of Sound and Vibration* 321 (2009) 184–200.
[4] J.D. Yau, Response of a maglev vehicle moving on a series of guideways with differential settlement, *Journal of Sound and Vibration* 324 (2009) 816–831.
[5] L.H. She, H. Wang, D.S. Zou, Z.Z. Zhang, W.S. Chang, Hopf bifurcation of maglev system with coupled elastic guideway, *Proceedings of the twentieth International Conference on Magnetically Levitated Systems and Linear Drives*, California, 2008.
[6] T.E. Albert, G. Oleszczuk, A.M. Hanasoge, Stable levitation control of magnetically suspended vehicles with structural flexibility, *Proceedings of the 2008 American Control Conference*, Washington, June 2008, pp. 4035–4040.
[7] J.P.Den Hartog, *Mechanical Vibrations*, fourth ed., McGraw-Hill, New York, 1956.
[8] X.M. Shi, C.S. Cai, Suppression of vehicle-induced bridge vibration using tuned mass damper, *Journal of Vibration and Control* 14 (7) (2008) 1037–1054.
[9] S.T. Wu, Y.J. Shao, Adaptive vibration control using a virtual-vibration-absorber, *Journal of Sound and Vibration* 305 (2007) 891–903.
[10] S.T. Wu, J.Y. Chen, Y.C. Yeh, Y.Y. Chiu, An active vibration absorber for a flexible plate boundary-controlled by a linear motor, *Journal of Sound and Vibration* 300 (2007) 250–264.
[11] S.T. Wu, Y.Y. Chiu, Y.C. Yeh, Hybrid vibration absorber with virtual passive devices, *Journal of Sound and Vibration* 299 (2007) 247–260.
[12] H.P. Wang, J. Li, K. Zhang, Non-resonant response, bifurcation and oscillation suppression of a non-autonomous system with delayed position feedback control, *Nonlinear Dynamics* 51 (2008) 447–464.
[13] T. Horiuchi, T. Konno, A new method for compensating actuator delay in real-time hybrid experiments, *Philosophical Transactions of the Royal Society of London A* 359 (2001) 1893–1909.
[14] K. Nikzad, J. Ghaboussi, S.L. Paul, Actuator dynamics and delay compensation using neurocontrollers, *Journal of Engineering Mechanics* (1996) 966–975.
[15] X.M. Dong, M. Yu, Z.S. Li, C.R. Liao, W.M. Chen, Neural network compensation of semi-active control for magneto-rheological suspension with time delay uncertainty, *Smart Material and Structures* 18 (1) (2009) 1–14.
[16] H.K. Khalil, *Nonlinear Systems*, third ed., Publishing House of Electronics Industry, Beijing, 2007.
[17] H. Elmali, M. Renzulli, N. Olgac, Experimental comparison of delayed resonator and PD controlled vibration absorbers using electromagnetic actuators, *Transactions of the ASME* 122 (2000) 514–520.
[18] E.R. Wechsler, Root locus algorithms for programmable pocket calculators, TDA Progress Report 42-73, 1983.
[19] P.A. Regalia, An improved Lattice-based adaptive IIR notch filter, *IEEE Transactions on Signal Processing* 39 (9) (1991) 2124–2128.